DINAME 2017 - Proceedings of the XVII International Symposium on Dynamic Problems of Mechanics
A. T. Fleury, D. A. Rade, P. R. G. Kurka (Editors), ABCM, São Sebastião, SP, Brazil, March 5-10, 2017

Monitoring of fatigue crack growth using a low-cost data acquisition device for impedance-based SHM considering dynamic measurements

Diogo de Souza Rabelo[1], Jared D. Hobeck[2], Daniel J. Inman[2], Roberto Mendes Finzi Neto[1], Valder Steffen Jr.[1]

[1] Faculty of Mechanical Engineering, Federal University of Uberlandia, Uberlandia, MG, Brazil. diogo.rabelo@ufu.br, finzi@ufu.br, vsteffen@ufu.br

[2] Aerospace Engineering Department, University of Michigan, Ann Arbor, MI, USA. jdhobeck@umich.edu, daninman@umich.edu

Abstract: A common problem in aircraft maintenance is the development of fatigue cracks in components located in areas of stress concentration. Although traditional nondestructive testing methods would be effective in inspecting cracks in an offline manner, real-time implementation of these methods is seldom accomplished. In this contribution, a procedure to monitor propagating cracks in aluminum beams undergoing dynamic cyclic loading is presented. A Piezoceramic (PZT) patch was attached to an aluminum sample to simultaneously excite the structure at a high-frequency range and monitor any changes in the structural mechanical impedance. To apply the fatigue load and induce fatigue crack, an electro-mechanical shaker was used. Proportional-Integral-Derivative (PID) controllers were used to change the shaker's drive frequency and drive acceleration in order to maintain the specimen under resonance in the first mode of vibration. During the vibrations, impedance measurements were acquired via the PZT patch by means of a low-cost impedance measuring device. Damage indexes were correlated with specific number of cycles until changes in drive frequency reached a critical limit. Finally, a statistical method is proposed to obtain the threshold for the Impedance-based Structural Health Monitoring (ISHM) system. The threshold is based on the knowledge of S/N curves and is compared with the damage indexes so that incipient damage could be detected before a visible crack could be observed in the specimen.

Keywords: Impedance-based SHM, Fatigue crack, Threshold determination

1. INTRODUCTION

Fatigue crack propagation in metallic structures is a persistent problem in many engineering structures and one of the most critical tasks in fatigue analysis is to reliably identify the crack at its initial stage (incipient crack). Furthermore, damage prognosis and diagnosis can be of utmost importance in military and civil applications such as aircraft fuselage, pipeline joints, rotating machinery, offshore oil platforms and other types of structures that operate in adverse environments or critical conditions. Failures should be located and repaired timely in order to minimize cost while maximizing system performance, safety, and reliability. Thus, the improvement of techniques that enhance the accuracy and reliability of the tracking process is highly desirable and is the subject of several studies both in academic and industrial contexts (Farrar et al., 2005).

In order to estimate the accumulated fatigue damage indirectly, a traditional way is to monitor loads or load sequences. This is what is commonly known as Operational Loads Monitoring (OLM). In aerospace structures, some of these methods include flight parameters-based loads monitoring and strain gauge based loads monitoring. However, experience accumulated over the last years leads to the conclusion that the vast amount of data collected needs a more efficient data management. This issue becomes specifically relevant when looking at the increasing in-service age of aircrafts. Furthermore, OLM systems are not able to directly detect and monitor structural damage. The OLM system can only provide a major input for analytically determining when damage might occur. Nevertheless, there is a gap between predicted and real damage that can be found as being two or three times higher than the values analytically predicted. This gap between predicted and real damage becomes even larger for composite materials where fatigue analysis and fracture mechanics studies of these materials is relatively less known as compared to metallic materials (Staszewski et al., 2004).

Most of the techniques under development operate on the actuator/sensor basis using smart material technology. The structural health monitoring (SHM) approach is fundamental not only for safety issues but also for minimizing downtime and decreasing maintenance costs. Among the techniques for monitoring the occurrence and propagation of structural damage, the impedance-based structural health monitoring has been shown to be a promising tool (Chaudhry et al., 1995; Giurgiutiu and Zagrai, 2000; Park and Inman, 2005; Rabelo et al., 2015a). The impedance method for SHM utilizes PZT patches as self-sensing actuators (Park et al., 2003). By measuring the electrical impedance, which depends on both the electrical properties of the transducer and the mechanical properties of the structure, incipient

damage can be detected.

Previous studies have demonstrated the possibility of using PZT patches for fatigue crack monitoring. For metallic materials, using impedance-based SHM techniques, Palomino et al (2011), show a correlation obtained between the number of cycles and the impedance signals by using meta-models. Cavalini et al. (2015) have used an impedance-based SHM system to detect incipient faults in rotating shafts using optimization techniques to normalize the data.

The ability to monitor structural integrity under operating conditions can be very helpful in engineering. In this paper, the impedance-based SHM system will be tested to detect crack initiation using impedance readings while the specimen undergoes continuous cyclic loadings. To accomplish this, an aluminum beam is coupled to an electromechanical shaker and measurements are performed in near real time. The goal of the present work is to investigate the conditions under which the impedance-based SHM method could be used to monitor a fatigue-induced crack and its propagation stages from continuous measurement conditions (without interruption). Additionally, a method for determining the crack threshold value is proposed as based on the use of S/N curves. A sensitivity analysis associated with the determined threshold value is performed using experimental data. For comparison purposes, results are also presented for a similar aluminum beam specimen where measurements were taken in a static condition at the same number of cycles and with the same loading specifications as the previous specimen.

2. FATIGUE FAILURE RESULTING FROM CYCLIC LOADING

Machine components are found to have failed under the action of repeated or fluctuating stresses. Yet, it has been observed that, under these conditions the actual maximum stresses were well below the ultimate strength of the material, or even below the yield strength. Fatigue failure may occur with no warning causing sudden, often catastrophic, damage and are therefore among the most dangerous failure modes. Three stages of fatigue crack development are commonly defined in the literature (Budynas and Nisbett, 2011). Stage I is the initiation of one or more micro-cracks due to cyclic plastic deformation followed by crystallographic propagation extending from two to five grains about the origin. Stage I cracks are not normally discernible to the naked eye. Stage II progresses from micro-cracks to macro-cracks forming parallel plateau-like fracture surfaces separated by longitudinal ridges. The plateaus are generally smooth and normal to the direction of maximum tensile stress. During cyclic loading, these crack surfaces open and close, rubbing together. Stage III occurs during the final stress cycle when the remaining material cannot support the loads, resulting in a sudden, fast fracture. Once a crack has been initiated in any surface, it propagates rapidly due to the high stress concentration.

In conventional fatigue/endurance testing, the results are presented in the form of plots of stress (applied alternating stress magnitude σ) versus the number of stress cycles Nc required to cause fracture, commonly referred to as S/N diagrams in the literature. In this paper, the beams used in the experiment are made of aluminum 6061-T6, which is a material that does not exhibit a well-defined endurance limit. In this case, it is customary to define the stress required to cause failure for a given number of cycles as the endurance limit σ_L. A Federal Aviation Agency (FAA) handbook, (2003) provides best-fit S/N curves for unnotched 6061-T6 aluminum alloy of various products (See figure 1):

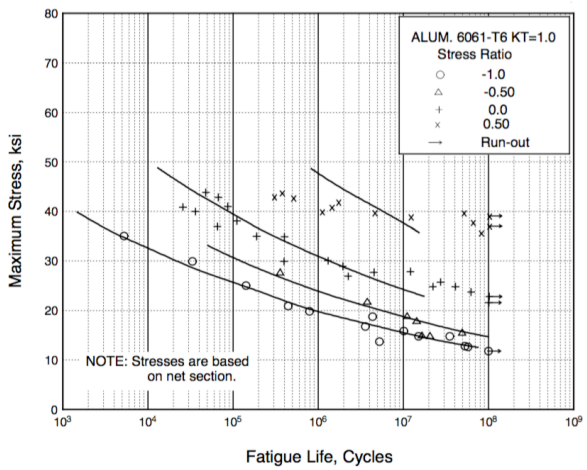

Figure 1 – Best-fit S/N curves for unnotched 6061-T^aluminum alloy, various wrought products, longitudinal direction. Adapted from (DOT/FAA/AR-MMPDS-01, 2003).

The S/N curve is often used to represent a 50 % probability of failure curve. This means that if a large number of fatigue specimens of one of the metals were tested at a given fatigue strength, approximately 50 % of the specimens would be expected to fail prior to Nc number of cycles of load corresponding to the given fatigue strength.

3. IMPEDANCE-BASED STRUCTURAL HEALTH MONITORING

The impedance-based structural health monitoring (ISHM) technique is considered as being a method of non-destructive evaluation. It utilizes electromechanically coupled properties of piezoelectric material (such as PZT) bonded to a structure such that the electrical impedance of the PZT becomes a function of the mechanical impedance of the structure. A PZT patch is bonded to (or embedded into) a structure and a high-frequency, low-amplitude electric voltage is applied, generating strain in the PZT. Strain in the PZT causes strain in the structure and the total structural response of the PZT/structure system generates a unique electrical impedance signature. In the case a structural modification occurs, such as damage, it can be observed as a change in the electric response of the PZT patch.

Damage leads to changes in the structure's mechanical impedance, thus modifying local dynamic features. Hence, the electrical impedance is measured in order to monitor the so-called health state of the structure, through a comparison with a previous baseline measure, i.e., the pristine condition. The real part of the electrical impedance is more reactive to damage since the imaginary part contains the capacitive portion of the PZT patch, which is more sensitive to temperature variation (Rabelo et al., 2015b). The curve that represents the impedance response provides a qualitative assessment of the damage. For a quantitative assessment of the failure, a previously defined Damage Metric (DM), or Damage Index (DI) is used. In the present contribution, the damage metric used is the correlation coefficient deviation (CCD). This DM uses two signals, where the first corresponds to the baseline and the second is the test measurement. Equation 1 provides the CCD:

$$CCD = 1 - \frac{1}{n}\sum_{i=1}^{n}\left\{\frac{\left[Re\left(Z_{1,i}\right) - Re\left(\bar{Z}_1\right)\right]\left[Re\left(Z_{2,i}\right) - Re\left(\bar{Z}_2\right)\right]}{S_{Z_1} S_{Z_2}}\right\} \tag{1}$$

where $\mathrm{Re}\left(Z_1\right)$ and $\mathrm{Re}\left(Z_2\right)$ are the real parts of the impedance of the baseline and test measurement at frequency i, respectively; n is the number of frequency points, $\mathrm{Re}\left(\bar{Z}_1\right)$ and $\mathrm{Re}\left(\bar{Z}_2\right)$ are the average of the baseline and test measurement, respectively; S_{Z_1} and S_{Z_2} are the standard deviations of the baseline and test measurements, respectively.

Impedance frequency ranges are commonly determined experimentally according to the density of peaks contained in a given range. Generally, impedance signatures are acquired at high frequencies in the range of 30-400 kHz. The wavelength of the excitation signal is closely related to the sensitivity and sensing area of the PZT.

As excitation frequency increases, the sensitivity also increases (Park et al., 2003). The drawback of increasing the frequency range too high is that usually the peak amplitudes tend to drop at higher frequencies and the sensor appears to have a smaller sensing area. Considering this trade-off is of significant importance while choosing the appropriate frequency range for successful ISHM implementation. In this paper, two frequency regions with good peak density but in different frequency regions are selected in order to verify the overall performance of the system.

3.1. Statistical threshold determination

The statistical threshold proposed in this work is obtained based on the theory of statistical process control (SPC). However, SPC requires an assessment of normality since it is assumed that the sample follows a Gaussian distribution. In order to test for normality, a Jarque-Bera (JB) test was performed with a confidence level of 99%. The JB test is a two-sided goodness-of-fit test suitable when a null distribution is unknown and its parameters have to be estimated. It uses the statistical moments of skewness and kurtosis for the normality assessment. Equation 2 expresses the test statistics:

$$JB = \frac{N}{6}\left[S_k{}^2 + \frac{\left(K_t - 3\right)^2}{4}\right] \tag{2}$$

where N is the sample size, S_k is the sample skewness, and K_t is the sample kurtosis. The hypotheses for the test are as follows:

- **H_0 (null hypothesis):** The sample follows a normal distribution.
- **H_1 (alternate hypothesis):** The sample does not follow a normal distribution.

Once normality is verified, SPC requirements are met and the threshold calculation can be performed. For a normal random variable, the population intervals corresponding to $\left[\mu - 2\sigma, \mu + 2\sigma\right]$ should fit 95.4% of all observations, where μ is the population mean and σ is the standard deviation. The threshold was estimated according to Equation 3:

$$T = \bar{x} + 2s \tag{3}$$

where $\bar{x}$ and s represent the sample mean and standard deviations, respectively.

The threshold defined in Equation 3 is equivalent to the Upper Control Limit (UCL) from traditional control charts used in SPC applications. While this approach might not seem to be particularly rigorous since the population parameters were estimated from the sample statistics, if more rigorous analysis is required confidence intervals can be used if desired (Rabelo et al., 2016). Additionally, measurement points in smaller number of cycles intervals or data from other specimens could be a way to increase the confidence of the inference process.

4. TEST SETUP AND EXPERIMENTATION

An electromechanical shaker was used in order to induce fatigue cracking in the aluminum beam. An accelerometer (model: 352C67) from PCB Piezotronics Inc. was attached to the base of the shaker in order to provide the excitation force acceleration. This accelerometer had a sensitivity of 9.94 mV/m/s2. The beam acceleration was measured using a Laser Doppler Vibrometer (LVD) from Polytec Inc. (Model: OFV-5000) with a sensitivity of 500 mm/s/V. The shaker was voltage driven by an amplifier controller with a computer through a NI USB-6211 data acquisition card (NI DAQ).

By exciting a beam at its first bending mode of vibration while controlling tip deflection, one can prescribe the maximum expected bending stress $\sigma_{\max}$ on the beam. This maximum stress is located at the base of the beam, which is where damage is expected to occur (Budynas and Nisbett, 2011). Given that the beam specimen was long, slender, and had uniform mass and stiffness properties it could be treated as an Euler-Bernoulli beam (Inman, 2013). The mode shape corresponding to the first bending mode of vibration for the beam was estimated using the deflection of the cantilevered beam subject to a uniformly distributed load along its length. Given this assumed mode shape, it was possible to determine the tip deflection y_{max} by measuring the deflection at any point along the beam with exception of the clamping location. By combining expressions for both deflection and bending stress, one can obtain the following relationship between maximum tip deflection and maximum stress:

$$y_{max} = -\frac{1}{2}\frac{l^2\sigma_{max}}{Et} \tag{4}$$

where l is the beam length, E is the modulus of elasticity and t is the thickness.

The phase angle between excitation force acceleration (A) and beam acceleration (B) vectors can be expressed as:

$$\Phi = arccos\left(\frac{A \bullet B}{\|A\| \cdot \|B\|}\right) \tag{5}$$

by taking advantage of the law of cosines where ($\bullet$) denotes the dot product and the vertical pairs of lines denote taking the norm of the corresponding vector.

The acceleration signals were used in a control routine that was designed in Labview® environment, where PID controllers were used to maintain the specimen under resonance (phase between excitation force and beam acceleration at 90 º) and at the desired stress level.

The aluminum beam made of 6061-T6 alloy had a width, thickness, and free length of 1 inch, 0.1226 inches, and 12 inches, respectively. The PZT patch was bonded 8 inches from the clamp. A small patch of reflective tape was positioned 3 inches from the clamp. A photo of the specimen is shown in figure 2:

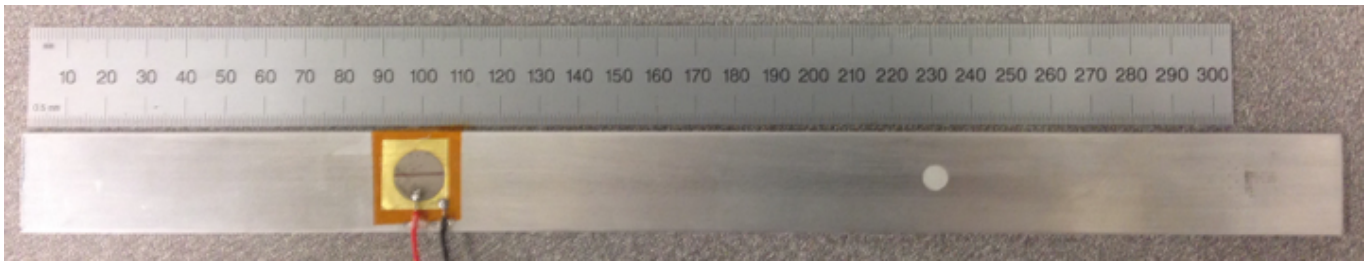

Figure 2 – Instrumented beam with PZT patch and reflective tape.

Based on typical S/N curves for aluminum 6061-T6 (figure 1), the fatigue strength chosen for the experiment was 150 MPa, with damage expected to initiate after approximately 500,000 load cycles. Preliminary tests were performed in order to determine the stress required to cause failure for a given number of cycles, i.e. the endurance limit stress σ_L. After preliminary tests, the desired stress amplitude and number of cycles were determined to be 150 MPa and 500k cyclic loads. Impedance measurements were taken from a round, 0.5-inch diameter, 0.0075-inch thick piezoceramic

disk (model: PSI-5A4E) from Piezosystems Inc. The PZT disk was bonded to one side of the specimen using a dual compound epoxy (type: DP460) from 3M Inc.

The impedance-measuring device used in the experiment has a 0.1 Ω resolution, and it was configured with 2048 averages per frequency point, impedance signatures were measured with 1000 frequency points. The architecture of the impedance-measuring device was developed and described by Finzi Neto et. al., (2011).

The test setup scheme is shown in figure 3(a) while the actual test setup is shown in figure 3(b). A shaker table was placed on top of the shaker so that the beam would be positioned on top of the shaker as well, with excitation forces being applied only at its base. Impedance measurements were made for frequency ranges of 28-48 kHz and 101-109 kHz. These two frequency ranges were experimentally chosen based on the good peak density observed in the impedance signatures.

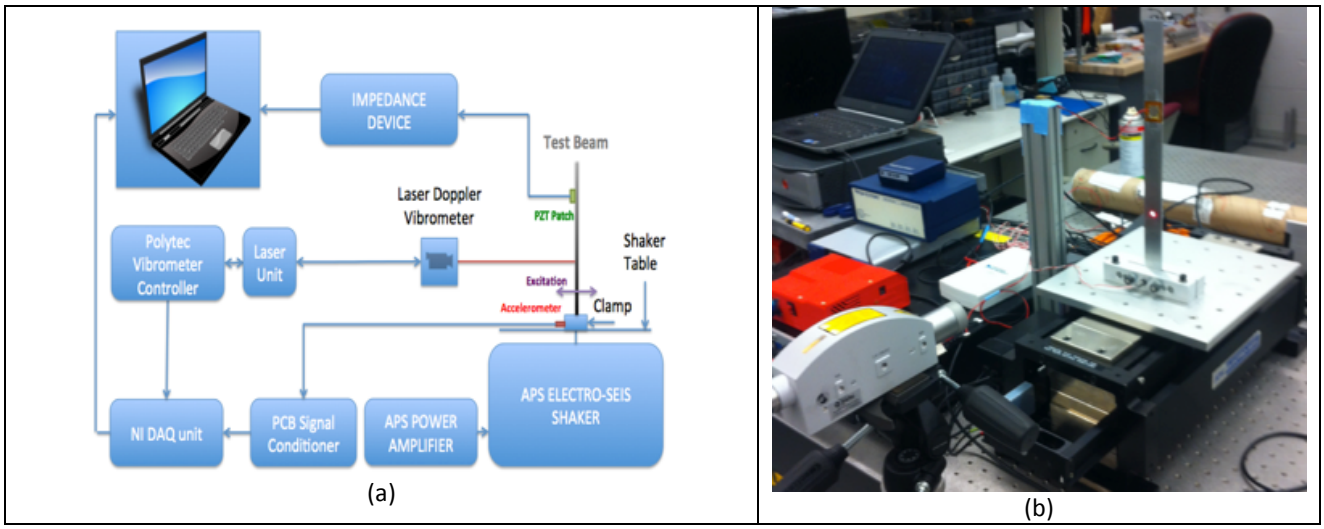

Figure 3 – Test setup (a) Scheme of experiment; (b) Actual test setup.

The flowchart shown in figure 4 illustrates various steps of the experimental procedure:

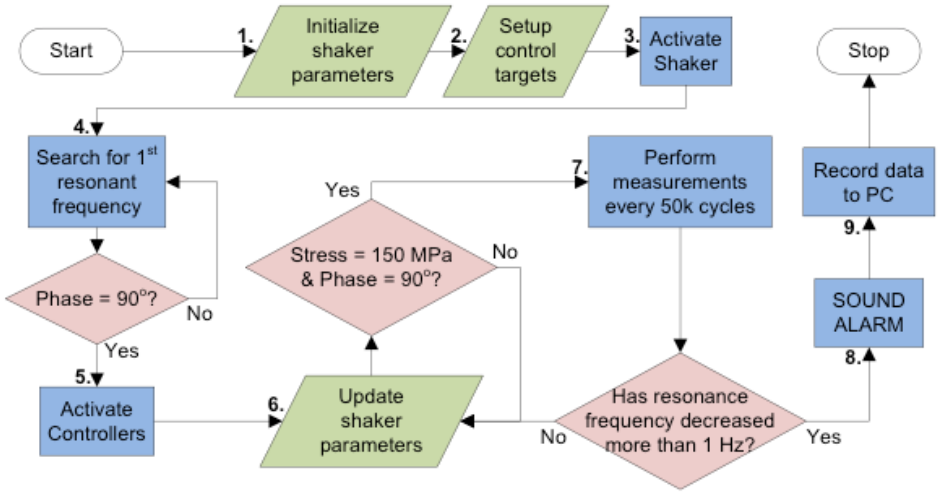

Figure 4 – Flowchart of experiment.

In figure 4, the first procedure, **Initialize shaker parameters**, configures the drive frequency and drive acceleration. In this procedure, a sinusoidal signal is generated in Labview® and sent to the NI DAQ. The signal is amplified and then applied by the shaker to the test beam. The next step, **Setup control targets**, aims to adjust control parameters like frequency gain, stress gain and the shaker's voltage amplitude gain. In the step **Search for 1st resonance frequency**, the frequency is found with a low amplitude vibration by searching the frequency at which the phase between the excitation force and beam acceleration is 90º, i.e., achieved resonance. At this point, the impedance baseline signature is recorded. The 1st resonance frequency is set and a stop criterion is programmed so that if the drive frequency decreases more than 1 Hz (effect of cracking), an alarm is activated. In step **Activate Controllers**, the phase target (90º) and stress target (150 MPa) are set. **Update shaker parameters** adjusts the drive frequency, drive acceleration and drive amplitude in order to maintain the beam under resonance (phase = 90º) and at the desired target stress. In the mean time, the values

of stress are recorded along with the phase, drive frequency, and number of cycles. This step is constantly active until the stop criterion is reached. Measurements are taken in step 7 for every 50k cycles reached. After the natural frequency has decreased more than 1 Hz in magnitude due to loss of stiffness, a safety alarm was sounded and final impedance readings were taken in step 9.

It should be noted that since damage was expected to initiate at 500k cycles, the cyclic loadings were interrupted after impedance measurements were taken in order to check for any visible cracks. This procedure was interrupted when the stop criterion was reached at 638k cycles. Additionally, although impedance signatures are generally sensitive to temperature variations in this experiment, temperature was assumed to have remained constant during testing.

5. RESULTS AND DISCUSSION

The acquisition time for each impedance measurement was approximately 28 seconds due to the averaging process and number of frequency points necessary to provide 8 Hz of frequency resolution. Hence, each test condition corresponds to the moment when the number of stress cycles reached the 50 k mark. The specimen's first resonance frequency was found to be 25.03 Hz.

It is worth mentioning that the baseline was acquired while the specimen was under cyclic loading, vibrating in the first resonance mode and with a lower stress level (20 MPa). All measurements were performed for the beam under vibration (cycling) condition. This procedure was adopted since there are significant variations between the impedance signatures taken with the beam at rest and the vibrating beam, as can be seen in figure 5a. Also, a 3rd order Savitsky-Golay FIR filter, set with 31 points for interpolation was applied to the data in order to remove partially the inherent noise and also to smooth the impedance curves (see figure 5b).

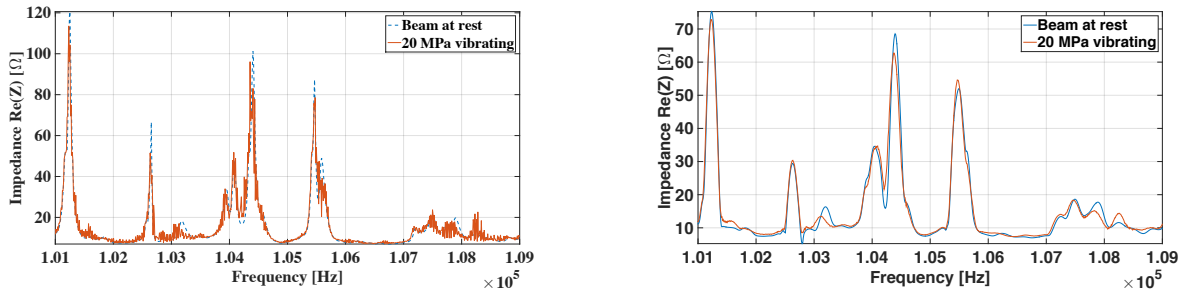

Figure 5 – Baseline comparison between motionless beam and vibrating beam. (a) Without filtering; (b) With Savitsky-Golay filtering.

No meaningful conclusion could be reached using the baseline corresponding to the beam at rest as compared to the test data obtained while the beam was vibrating. Impedance readings taken under cyclic loading presented the oscillatory behavior around the peaks as presented in figure 5a. A qualitative assessment of the fatigue test provided by the impedance-based SHM method is shown in figure 6 by using only impedance readings with the specimen vibrating.

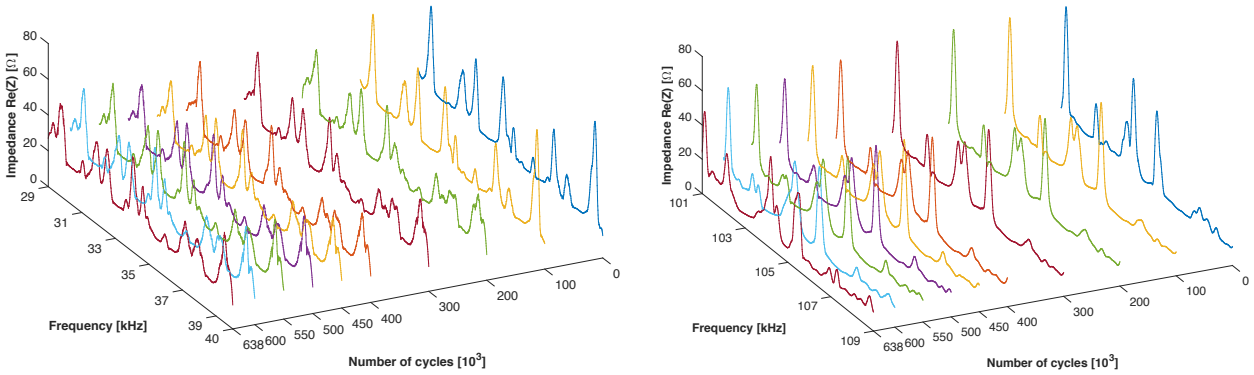

Figure 6 – Impedance signatures with beam vibrating: (a) 29-40 kHz; (b) 101-109 kHz.

Figure 6 show that, as the number of cycles progresses, the impedance signatures become more different from the baseline (0 cycles reference), for the beam at rest and beam vibrating, respectively. These changes will be used to determine the severity of damage (or crack propagation) occurring in the specimen tested. It should be noted that some of the impedance responses (for 50, 150, and 350 cycles) are not shown in the figure for the sake of clarity. In addition, the length of the specimen was measured before and after the loading, and no residual strain was noticeable.

5.1. Analysis and statistical threshold determination

As previously mentioned, the load cycle was interrupted after impedance measurements at 500k, 550k and 600 k cycles for visual inspection. The alarm was activated at 638k cycles as the resonance frequency decreased more than 1 Hz. At this point, the final impedance measurement was collected and a visible crack could be seen at the opposite side of the PZT patch. Figure 7(a) shows that the crack was generated at the clamped end and figure 7(b) zooms and filters the image for better visualization of the crack.

the impedance-based SHM method is shown in figure 6 by using only impedance readings with the specimen vibrating.

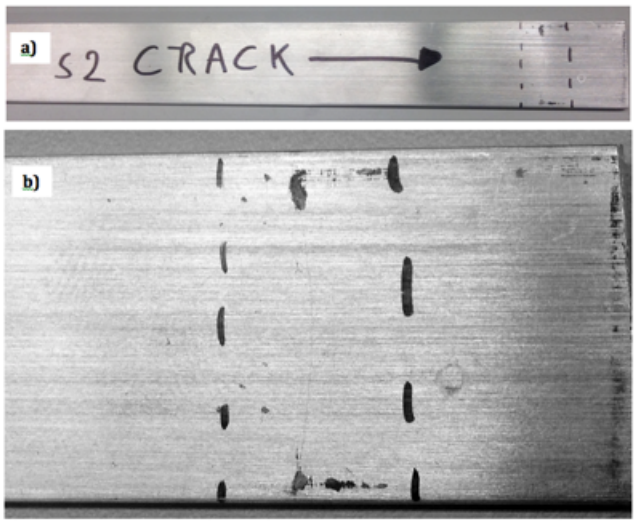

Figure 7 – Beam specimen with (a) crack location and (b) detailed view.

Calculating the CCD (Equation 2) with the impedance curves of figure 6a and figure 6b, damage indices for each structural condition, i.e., for each number of cyclic loads considered, were attained. A bar chart that compares the baseline to each structural condition was used to show the damage indices graphically as presented in figure 8a and figure 8b.

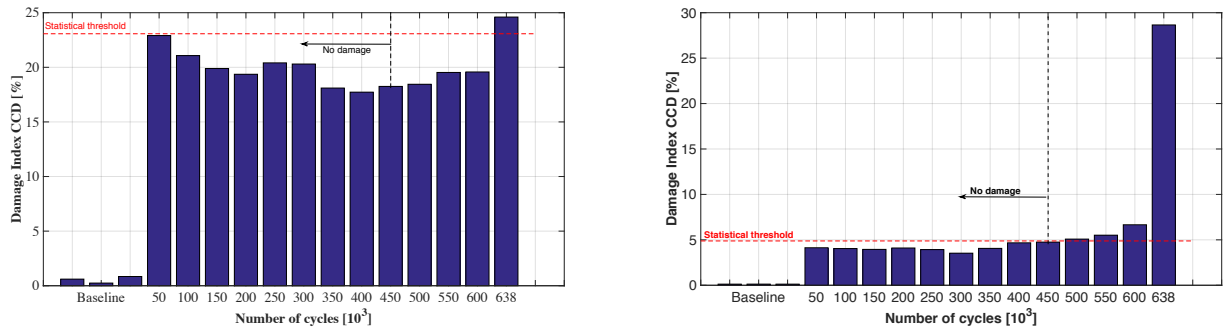

Figure 8 – The CCD damage indexes of the beam as a function of the number of cycles. (a) – (29 to 40 kHz); (b) – (101 to 109 kHz).

The first three bars in the plots of figure 9 compare the baselines. The statistical thresholds in figure 9 were

determined from the S/N curve for aluminum 6061-T6. As S/N curves represent 50% probability of failure prior to the number of cycles to fail, the procedure adopted to estimate the threshold considered the damage indices from 50k cycles to 450k cycles. This group of values was considered the "no damage" sample. It was assumed that this data was random since according to the S/N estimation, no damage has occurred up to this point and therefore the damage indices should not have significant variations. The damage index results up to 450k cycles indicate that the crack nucleation was not fully developed at this point since no significant variations in the indices is found. The normality assessment is presented in Table 1, where the results were obtained by using the statistics toolbox from MATLAB®

Table 1 – Normality Assessment results for the "no damage" condition sample.

Confidence-Level	p-value	JB	Crit. Val.	H
99%	0.5	0.1675	5.0988	0

The H value equal to zero in Table 1 means that the null hypothesis should not be rejected with 99% confidence. It should be noted that the assumption that the "no damage" sample is random and normal is important, considering that the sample is small, containing only 9 values.

As can be seen in the results shown in figure 8a, the frequency range of 29-40 kHz was only able to detect damage at the final stage of the test (when resonance frequency has decreased more than 1 Hz, at 638 kHz). However, the frequency range of 101-109 kHz provides much better results (see Fig. 8b), considering that the damage indices from 500 kHz to 638 kHz have an increasing trend and are all above the statistical threshold. These results indicate that crack nucleation was detected and the higher frequency range is more appropriate for sensing incipient damage. No visible crack appeared in the specimen before the natural frequency changed significantly. The sudden jump in the damage index between 600 kHz and 638 kHz indicates the transition state from micro-cracks to visible macro-cracks.

6. CONCLUSION

A statistical method to determine the threshold level for fatigue crack detection in metallic structures using impedance-based structural health monitoring was proposed. The method uses information from the S/N curve for a metallic material and takes into account the fatigue stress level and the expected number of cycles for damage initiation. Impedance signatures were acquired continuously while the structure was submitted to cyclic loadings (acquisition without interruption). Additionally, this paper shows that although two frequency ranges exhibited good peak density, the higher frequency range presented better sensitivity for the detection of incipient damage. Thus, as frequency increases, sensitivity also increases and damage of smaller severity can be detected. However, another effect that is present as the monitoring frequency band increases is that the peak amplitudes of the impedance readings decrease. As a consequence, the radius of sensitivity could be reduced. This can be observed when changes in the boundary conditions are perceived, since typically the lower frequency bands are more sensitive to these changes. Adversely, when incipient damage is present, the higher frequency bands are the most sensitive.

With the threshold value obtained, a fatigue crack could be detected successfully before being visible to the naked eye, using a higher frequency range. It should be pointed out that the impedance signals considered in the present work were obtained under dynamic conditions, which is extremely desirable for real-time monitoring of engineering structures while in their operational condition. However, the fatigue testing was done in a laboratory environment with a shaker producing stress cycles with constant amplitude. In real world applications of engineering structures, fatigue damage might occur in situations where the stress variations are not of constant amplitude. Further studies are scheduled involving complex structures to evaluate different types of fatigue conditions in metallic and composite materials.

7. ACKNOWLEDGEMENTS

The authors are thankful to the Brazilian research agencies CNPq and CAPES through the (INCT-EIE) and also to FAPEMIG for the financial support provided for the research effort.

8. REFERENCES

Farrar CR, Lieven NAJ, Bement MT (2005) An Introduction to Damage Prognosis. *Damage Prognosis for Aerospace, Civil and Mechanical System*, Wiley, Chap. 1, pp. 1-12.

Staszewski WJ, Boller C, Tomlinson GR (2004) *Health Monitoring of Aerospace Structures: Smart Sensor Technologies and Signal Processing*, John Wiley & Sons, Chap. 2, pp. 47-53.

Chaudhry Z, Joseph T, Sun F, Rogers C (1995) Local-Area Health Monitoring of Aircraft via Piezoelectric Actuator/Sensor Patches. In: *Proceedings of the SPIE Vol. 2443 – Conference Smart Structures and Integrated Systems* San Diego, CA, USA.

Giurgiutiu V and Zagrai A (2000) Characterization of Piezoelectric Wafer Active Sensors, *Journal of Intelligent Material Systems and Structures*, 11(12): 959-976.

Park G and Inman DJ (2005) Impedance-Based Structural Health Monitoring, *Damage Prognosis for Aerospace, Civil and Mechanical System*, Wiley, Chap. 13, pp. 1-12.

Rabelo DS, Finzi Neto RM, Steffen Jr. V (2015) Impedance-based Structural Health Monitoring incorporating compensation of temperature variation effects. In: *Proc. of the 23rd ABCM International Congress of Mechanical Engineering*. Rio de Janeiro, Brazil.

Rabelo DS, Steffen Jr. V, Finzi Neto RM, Lacerda HB (2015) A statistical approach for assessing reliability for impedance-based structural health monitoring. In: *Proc. of the 10th International Workshop on Structural Health Monitoring*, Stanford University, Palo Alto-CA, USA.

Park G, Sohn H, Farrar CR, Inman DJ (2003) Overview of Piezoelectric Impedance-Based Health Monitoring and Path Forward, *The Shock and Vibration Digest*, 35(6): 451-463.

Palomino LV, Moura Jr. JRV, Tsuruta KM, Rade DA, Rade DA, Steffen Jr. V (2011) Impedance-based health monitoring and mechanical testing of structures, *Smart Structures and Systems*, 7(1): 15-25.

Cavalini Jr. AA, Oliveira DD, Rabelo DS, Finzi Neto RM, Steffen Jr. V (2015) Fault Detection in a rotating shaft by using the electromechanical impedance method and a temperature compensation approach. In Proc. of the XXXVI Ibero-Latin American Congress on Computational Methods in Engineering – CILAMCE 2015, Rio de Janeiro – Brazil.

Budynas RG and Nisbett JK (2011) *Shigley's Mechanical Engineering Design, 9th ed.*, McGraw-Hill, Chap. 6-3, pp. 71-272.

DOT/FAA/AR-MMPDS-01: (2003) *Metallic Material Properties Development and Standardization*, Department of Transportation, Federal Aviation Agency, January 2003, USA.

Rabelo DS, Steffen Jr. V, Finzi Neto RM, Lacerda HB (2016) Impedance-based structural health monitoring and statistical method for threshold determination applied to 2024-T3 aluminum panels under varying temperature, *Structural Health Monitoring*, 15(1) 1-17.

Inman DJ (2013) *Engineering Vibration, 4th Edition*. Pearson, Chap. 6, pp. 431-469.

Finzi Neto RM, Steffen Jr. V, Rade DA, Gallo CA, Palomino LV (2011) A low-cost electromechanical impedance-based SHM architecture for multiplexes piezoceramic actuators. *Structural Health Monitoring*, 10(4): 391-401.

9. RESPONSIBILITY NOTICE

The authors are the only responsible for the material included in this paper.